Heterogeneous Hydrogel Structures with Spatiotemporal Reconfigurability using Addressable and Tunable Voxels

Roozbeh Khodambashi† Yousif Alsaid† Rossana Rico Matthew M. Peet Hamid Marvi Rebecca E. Fisher Spring Berman Ximin He* Daniel M. Aukes*

R. Khodambashi, Dr. D. M. Aukes
The Polytechnic School, Fulton Schools of Engineering, Arizona State University, Mesa, AZ, 85212, USA
E-mail: danaukes@asu.edu, rkhodamb@asu.edu
Y. Alsaid, R. Rico, Dr. X. He
Department of Materials Science and Engineering, University of California Los Angeles, Los Angeles, California, 90095, USA
E-mail: ximinhe@ucla.edu
Dr. Rebecca E. Fisher
Department of Basic Medical Sciences, University of Arizona College of Medicine-Phoenix, Phoenix, AZ 85004, USA
School of Life Sciences, Arizona State University, Tempe, AZ 85287, USA
Dr. H. Marvi, Dr. M. M. Peet, Dr. S. Berman
School for Engineering of Matter, Transport and Energy, Arizona State University, Tempe, AZ 85281, USA

Keywords: *heterogeneous hydrogel structures, soft voxel actuators, tunable hydrogel properties, on-demand shape morphing, reconfigurable hydrogel robots*

Abstract

Stimuli-responsive hydrogels can sense environmental cues and change their volume accordingly without the need for additional sensors or actuators. This enables a significant reduction in the size and complexity of resulting devices. However, since the responsive volume change of hydrogels is typically uniform, their robotic applications requiring localized and time-varying deformations have been challenging to realize. Here, using addressable and tunable hydrogel building blocks – referred to as Soft Voxel Actuators (SVAs) –heterogeneous hydrogel structures with programmable spatiotemporal deformations is presented. SVAs are produced using a mixed-solvent photopolymerization method, utilizing a fast reaction speed and the cononsolvency property of PNIPAAm to produce highly interconnected hydrogel pore structures, resulting in tunable swelling ratio, swelling rate, and Young's Modulus in a simple, one-step casting process that is compatible with mass production of SVA units. By designing the location and swelling properties of each voxel and by activating embedded Joule heaters in the voxels, spatiotemporal deformations are achieved which enables heterogeneous hydrogel structures to manipulate objects, avoid obstacles, generate traveling waves and morph to different shapes. Together, these innovations pave the way towards tunable, untethered, and high degree-of-freedom hydrogel robots that can adapt and respond to changing conditions in unstructured environments.

Introduction

Smart hydrogels have attracted great interest in many different fields, such as drug delivery [1, 2], microfluidics [3, 4], and soft robotics [5], owing to their large and reversible volume changes in response to a broad range of stimuli without using any additional sensors and actuators. This feature helps reduce the size of devices made of smart hydrogels. Practical soft robotic applications, ranging from basic bending and shortening primitives to complex reconfigurations, all require time-varying and local deformations of bulk hydrogels in order to approach the dexterity of soft organisms in performing tasks such as grasping and manipulation [6, 7]. However, the responsive volume change of smart hydrogels is typically uniform. Two main approaches have been adopted by researchers to achieve nonuniform spatiotemporal deformation in hydrogels [6]. In the first approach, heterogeneous structures in the shape of sheets and rods are fabricated by patterning material domains using manufacturing techniques such as micro- and meso-patterning [8, 9, 10, 11, 12, 13] and 3D printing [14]. Differing swelling properties of neighboring domains upon stimulation results in nonuniform strain fields in these structures, causing them to transform into a variety of

complex shapes like coils and conical helices [15, 16]. The range of compatible materials available for each domain, however, is often limited by practical fabrication constraints, such as ink viscosity for 3D printing [14]. Moreover, the geometry and material selected for each domain determine the shape transformations; these features cannot be changed after manufacturing, making on-demand reconfiguration infeasible.

The second approach towards achieving nonuniform spatiotemporal deformations uses an inhomogeneous or time-varying stimulus, such as patterns of structured light [17], local irradiation by near-infrared light [18], or localized electric fields [19]. In these methods, the hydrogel material itself is typically homogeneous, but the stimulus intensity varies across different regions, causing localized and time-varying deformations. These techniques, while suitable for on-demand shape reconfiguration, often require bulky external equipment, ultimately leading to challenges in mobile robot applications.

Nature has adopted a hierarchical approach in addressing these challenges by using motor units as building blocks for heterogeneous muscle tissue demonstrating complex spatiotemporally reprogrammable deformations [20, 21]. A motor unit consists of a motor neuron and the muscle fibers innervated by its axonal terminals [22]. It behaves as a stimuli-responsive building block, producing unidirectional deformation in response to electrical stimulus from the central nervous system (CNS). The variations in orientation [23] and response rate [24] of muscle fibers create the structural heterogeneity [25] required for nonuniform hard-coded deformations; the on-demand control over location and intensity of the electrical stimulus provides the spatiotemporal reprogrammability [26, 27, 28].

Virtual voxels have been used for decades as building blocks to represent shapes in 3-D space for computer graphics applications [29]. More recently, voxel-based simulations have been used to predict bulk material properties of structures – including structures made of smart hydrogels – by controlling the material properties of individual virtual voxels [30, 31, 32]. Virtual voxels have also been utilized to simulate heterogeneous structures with robotic functions [33]. However, physical realization of voxels as building blocks have been limited to passive and often rigid materials, and are used in conjunction with additive manufacturing processes to increase their throughput [34]. One recent work has used voxel-based computer simulations to optimize the distribution of active and passive materials in a structure for achieving different goals and the resulting mechanisms are physically realized using cardiomyocytes from a frog as building blocks for creating responsive structures[35].

Inspired by nature's approach for achieving on-demand spatiotemporal deformations in muscle tissue, we introduce addressable and tunable building blocks that can be assembled to create heterogeneous hydrogel structures with *hard-coded* or *reprogrammable* shape change. These building blocks, herein referred to as soft voxel actuators (SVAs), are shown in **Figure 1**-A, left. The SVA units, consisting of a responsive hydrogel material and corresponding electrical connections, are inspired by the motor units of muscle tissue (Figure 1-A, right). The deformation of SVA units as a result of an electrical stimulus from a microcontroller unit (MCU) is analogous to the contraction of muscle fiber units in response to stimuli from the central nervous system (CNS). The selection of electrical stimuli as opposed to other types of stimuli is advantageous, since it enables addressing SVAs directly by small-footprint microcontrollers without the need for bulky equipment or human intervention. [36].

Results

Two types of SVAs have been realized and are described herein: one without an embedded heater (referred to as SVA-I), and one with an embedded heater (referred to as SVA-II), as shown in Figure 1-B. Various combinations of SVA-I and SVA-II can be used for designing and fabricating heterogeneous assemblies. One possible combination, shown in Figure 1-B(i), uses SVA-I to create pre-programmed voxel assemblies. Based on the specific arrangement of SVA-I consisting of different swelling properties (mainly volume

change ratio and rate), complex deformations can be demonstrated. These SVA assemblies deform in response to regular and repeated homogeneous temperature changes (such as the bulk heating and cooling of a water reservoir), generating motions without the need for an on-board energy source. It should be noted that hydrogels expand and contract based on the diffusion of water into and out of their structure when the temperature is passed their critical transition temperature which is around 32° C in case of PNIPAAm hydrogels. Therefore, all our experiments are performed in a water bath. Another combination of SVAs shown in Figure 1-B(ii), uses thick film surface mount (SMD) resistive elements with a resistance of 10 ohms as Joule heaters in SVA-II units to create time-varying and inhomogeneous temperature fields, resulting in on-demand dynamic deformations and real-time reconfigurability. Details of the Joule heater elements are presented in the Supporting Information.

The ability to select from a broad range of material properties for SVA fabrication can expand the design space of resulting heterogeneous structures. Therefore, a synthesis method that can tune the ratio and rate of hydrogel volume change is required. A variety of physical and chemical methods have been explored to alter the swelling properties of hydrogels [37, 38]. These methods are limited by factors such as the narrow range of achievable swelling properties [39, 40], large trade-offs in mechanical properties [41, 42], long processing times [8, 43], and a need for careful control of synthesis conditions such as temperature [44] and precursor additives [45].

We take advantage of PNIPAAm's cononsolvency, a property of reduced solvation in a mixture of two solvents due to a delicate balance between polymer-solvent and solvent-solvent interactions [46]. Employing a water and dimethyl sulfoxide (DMSO) mixed solvent in the PNIPAAm hydrogel precursor solution, followed by rapid photopolymerization to induce interconnected open pores, significantly enhanced the rate of water transport into and out of the hydrogel matrix and thus the actuation speed. The microstructure of the gel is altered by changing the water volume fraction (φ_w) in the mixed water/DMSO solvent. The SVA swelling rate and displacement, which are directly related to its hydrogel microstructure, are therefore tuned by merely adjusting φ_w. Polymerization solvent composition is known to affect the swelling properties of the synthesized PNIPAAm hydrogels [47, 48, 49, 50, 51]. The combination of the mixed solvent method with a fast 15 s photopolymerization step is critical for inducing and fixing local aggregations of polymer chains in place, resulting in PNIPAAm hydrogels with open pore structures (**Figure 2**-A(i)). Such open pore structures exhibit significantly enhanced rates of thermoresponsive volume change in both heating and cooling phases, compared to conventional hours-long mixed solvent thermopolymerization methods (control experiment), in which the precursors are constantly diffusing towards a homogeneous molecular equilibrium throughout the duration of the reaction, leading to a less interconnected pore structure with thicker pore walls (Figure 2-A(ii)). In order to ensure a valid comparison, the recipe for a representative thermopolymerized control hydrogel was carefully tuned using the initiator concentration while leaving all other components of the precursor solution unchanged, choosing a reaction time such that the conversion and water content match those of the photopolymerized hydrogel (Supporting Information and Table S2). It is readily observed that with equivalent water content, reaction conversion, and reaction solvent composition, the thermopolymerized hydrogel deswells as fast as the photopolymerized hydrogel Figure 2-B(i) and the two reach nearly identical shrunken volumes (Figure S8, Supporting Information). However the reswelling speed of the thermopolymerized control sample is ∼25 times slower than the photopolymerized sample, which can be attributed to the lower observable tortuosity present in the photopolymerized sample Figure 2-B(ii). The Young's Modulus of the thermopolymerized hydrogel is ∼10 times higher than that of the photopolymerized one (Figure S9, Supporting Information).

The effect of varying φ_w on the hydrogel microstructure has been investigated by scanning electron microscopy (SEM), as shown in Figure 2-C. Six hydrogels consisting of various φ_w were synthesized; they are each represented by a character code ranging from HG00 (representing a hydrogel with $\varphi_w = 0.0$) to HG05 (representing a hydrogel with $\varphi_w = 0.5$). Details of the SEM imaging procedure are described in the Supporting Information. Distinct changes in the microstructure can be observed as a function of

φ_w, which impacts a variety of other material properties. When φ_w is increased from 0.0 to 0.2, pore size decreases and the pore wall surface begins to change from smooth to rough. We define $\varphi_w = 0.2$ as a critical water volume fraction, at which the microstructure of the gel starts to change from a closed-pore to an open-pore structure. SEM images for other values of φ_w are presented in Figure S4 in the Supporting Information. The changes in hydrogel microstructure play a role in the dynamic response of SVAs. The linear displacement generated by a SVA unit is measured using a vision-based test setup as described and shown in the Supporting Information and Figure S3. Figure 2-D plots the time evolution of the displacement (D) of SVA units with different values of φ_w as each SVA's embedded heater is turned on for 60 s and then turned off for 60 s. The displacement over time of the hydrogel made with $\varphi_w = 0.0$ is included as the basis for comparison across all tests. The negative displacement observed is because the SVAs initially expand instead of contract as the heater is turned on which might be due to water slightly expanding and vaporizing. Two performance criteria for the SVA units, deformation rate (DR) and maximum displacement (MD), are extracted from the data in Figure 2-D and are shown in Figure 2-E,F respectively. During both heating and cooling, DR is small for $\varphi_w < 0.2$. At $\varphi_w = 0.2$, the DR during heating is more than 36 times the DR during cooling. As a result, fast and large deformations are observed during the 60 s of heating, and almost no deformation is observed during the 60 s of cooling. Highest DR (in both heating and cooling) occurs in gels with $\varphi_w = 0.3$, while MD peaks at $\varphi_w = 0.2$ and decrease thereafter. In addition to swelling properties, other mechanical properties such as Young's modulus and force produced by the SVAs can also be tuned by adjusting φ_w (Figure S5, Supporting Information).

A variety of heterogeneous structures can be produced that transform into different configurations, depending on their hard-coded material domains, as shown in **Figure** 3. As a first example, a beam with only two material domains is fabricated from HG00 and HG02 hydrogels (Figure 3-A(i)). At 20 °C, the beam is in its equilibrium position. As the temperature increases to 45 °C, the HG02 hydrogel shrinks more than HG00 (from Figure 2-C,D, both MD and DR are higher for HG02), which results in a stress mismatch. To balance these stresses, the beam bends into a circular shape. We will henceforth refer to this structure as a 'gripper'. A second example uses HG00 and HG02 hydrogels again, but this time with 8 material domains, as shown in Figure 3-B(ii-iv). The beams in these figures consist of different arrangements of HG00 and HG02 voxels, and as a result exhibit different deformations when subjected to a homogeneous temperature change in the surrounding water from 20 °C to 45 °C (for details, see Movie S1 in the Supporting Information)

Patterning material domains can be used to leverage the shape transformations into unique functions tied to structural heterogeneity. To demonstrate this *structure–function* relationship, two different structures, Str-I and Str-II, are made with different combinations of HG00, HG02, and HG03, as shown in Figure 3-B. These structures represent a combination of the structures in Figure 3-A(i,ii). In response to a global cyclic temperature change from 20 °C to 45 °C and back to 20 °C, these structures are observed to bend towards an object, grasp it (by wrapping around it), and transport it to another location (Figure 3-B and (Movie S2, Supporting Information). The geometric configuration of material domains in both structures are the same. However, the 'gripper' portion of Str-I is a combination of HG00/HG03 domains, whereas in Str-II it is a combination of HG00/HG02 domains. As a result of this minor material difference, the object grasped by Str-I and Str-II moves along different trajectories, as seen in Figure 3-C, despite an identical set of initial conditions. Due to the high DR of HG03 during the cooling phase (Figure 2-E), the gripper in Str-I opens and the object is released in the early stages of the cooling phase. The gripper in Str-II, on the other hand, does not open at the same time as Str-I and continues to hold the object throughout its cooling phase; this can be attributed to the lower DR of the HG02 layer compared to HG03. To illustrate these differences, the x and y coordinates of the object over time are plotted in Figure 3-D, and the time when the object is released by each structure is indicated. Achieving inhomogeneous deformations in response to a homogeneous global stimulus using structures with hard-coded deformations as described simplifies the system and eliminates the need for on-board power sources.

For applications in dynamic, unstructured environments, such as underwater robotic exploration, it is less useful to pre-program complex trajectories into a structure, since global stimulus control is not always feasible. To enable on-demand thermoresponsive shape morphing in these conditions, SVA-II units may be employed, as depicted in Figure 1-B(ii). The 40×11×5 mm structure shown in **Figure 4**-A was assembled using 16 SVA-II units. These SVAs are made of HG03, which exhibits the highest DR observed across all recipes (Figure 2-E). The first example of on-demand shape morphing is illustrated in Figure 4-B(i), in which the structure morphs into an 'S' shape and a 'reverse S' shape when particular SVAs are actuated via commands from a microcontroller. A second example of on-demand shape morphing is illustrated in Figure 4-B(ii); it highlights how the curvature of a structure may be varied as a function of the voltage supplied to the SVA-II units.

Moving from static to dynamic on-demand shape changes requires time-varying activation of SVAs. As demonstrated in Figure 4-C, the choice of SVA actuation pattern can influence the end-effector trajectory of a structure. In this experiment, SVAs 1 thorough 8 are activated according to patterns denoted by P1 and P2. Each SVA is activated with maximum voltage (3.7 V) for 15 s before the next SVA is activated, as shown in Figure 4-C and Movie S3 in the Supporting Information.

While complex motion of SVA-II-based structures may be achieved using simple on (3.7 V) and off (0 V) activation signals, as discussed, intermediate voltages may also be applied to further enhance the complexity of shape change in soft heterogeneous structures. To demonstrate this, phase-shifted sinusoidal voltages were used as activation signals to generate longitudinal traveling waves in the structure. A pair of SVAs (comprising a SVA on the left and its adjucent SVA on the right) are activated using the same sinusoidal signal; SVAs 4 and 12 were not activated, to serve as a geometric reference point. The sinusoidal voltages applied to every SVA pair were $\frac{\pi}{8}$ rad out of phase with the voltages applied to its nearest active SVA pair. As an example, sinusoidal signals for four SVA pairs are shown in Figure 4-D. A contraction wave was formed as a result of this input signal pattern and traveled along the length of the structure, as illustrated in Figure 4-E. Movie S4 in the Supporting Information shows in detail how these waves are generated and propagated along the structure. Every point on the structure oscillates in a sinusoidal manner as the wave passes through it. The midpoint of the inactive SVA pair, which is highlighted by a yellow square in Figure 4-E, is shown as a reference point on the structure. Additionally, by sending the sinusoidal signals to SVAs located on only one side of the structure, for example SVAs 1 through 8, transverse traveling waves were generated in the structure (Movie S4, Supporting Information). The ability to control the trajectory of the structure's end-effector, as shown in Figure 4-C, is essential to successful functioning of the device in unstructured environments, in which working conditions may change during operation. As depicted in Figure 4-F, time-sequenced switching of selected SVA-II units within the structure makes it possible to accomplish various robotic tasks such as collision avoidance (top row) and object transport (bottom row). The trajectory of the end point p and the angle θ of the end plate over time (p and θ are defined in Figure 4-A) during each of these two tasks is displayed in Figure 4-G. The on-demand control of reorientation and translation of the end-effector made it possible to complete these two tasks, indicating that highly redundant time-varying deformations in heterogeneous structures are achievable using individually addressable SVA-II units (Movie S5, Supporting Information).

Conclusions

To summarize, we have developed the following tools to increase the variety and complexity of shape transformations in heterogeneous hydrogel structures: a voxel-based assembly design for patterning material domains, and a unique mixed-solvent photopolymerization hydrogel synthesis method for tuning swelling properties of the voxels. These tools offer a higher number of design parameters, namely, the configuration of the voxels, the material properties of each voxel, and the activation voltage of each voxel (in the case of SVA-II). This rich set of design parameters can be specified to build structures that meet the requirements of a variety of tasks. The resulting heterogeneous structures can generate complex time-varying trajectories

and traveling waves, enabling them to interact with unstructured environments in ways that could not be realized in bulk hydrogels or that would require sophisticated integration and manufacturing.

The simplicity of these tools advances the utility of hydrogel structures in robotics applications in a meaningful way because they can be used in robotics research laboratories that lack sophisticated material processing facilities. While this paper focuses specifically on PNIPAAm hydrogel voxels, soft and rigid voxels made of other types of responsive or non-responsive materials can also be incorporated into heterogeneous assemblies. Closed-loop control of the deformation of the structures presented in this paper could be achieved by integrating strain- and force-sensitive voxels, made of similar functional hydrogels, that serve as sensors. In addition, multi-objective optimization across material properties and voxel configurations can be used to design structures with higher force production capacity and energy efficiency. Currently, integrating multiple active degrees of freedom (DOFs) in miniaturized soft robots is challenging due to space limitations. Each SVA can be considered as an active DOF and we have demonstrated that the integration of a high number of SVAs in a small footprint, such as the 16-voxel structure presented in this paper, is possible. To address the challenges of fabricating large-scale assemblies consisting of hundreds of voxels, automated methods must be developed for scalable manufacturing and assembly of voxels.

Supporting Information
Supporting Information is available from the Wiley Online Library or from the author.

Acknowledgements
R.K. and Y.A. contributed equally to this work. The authors would like to thank Dongting Li for his help in image processing. This work was supported by Office of Naval Research (ONR) Award N00014-17-1-2117.

References

[1] N. Annabi, A. Tamayol, J. A. Uquillas, M. Akbari, L. E. Bertassoni, C. Cha, G. Camci-Unal, M. R. Dokmeci, N. A. Peppas, A. Khademhosseini, Advanced Materials **2014**, 26, 1 85.

[2] M. A. Stuart, W. T. Huck, J. Genzer, M. Müller, C. Ober, M. Stamm, G. B. Sukhorukov, I. Szleifer, V. V. Tsukruk, M. Urban, F. Winnik, S. Zauscher, I. Luzinov, S. Minko, Nature Materials **2010**, 9, 2 101.

[3] L. D'Eramo, B. Chollet, M. Leman, E. Martwong, M. Li, H. Geisler, J. Dupire, M. Kerdraon, C. Vergne, F. Monti, Y. Tran, P. Tabeling, Microsystems & Nanoengineering **2018**, 4, 1 1.

[4] C. B. Goy, R. E. Chaile, R. E. Madrid, Reactive and Functional Polymers **2019**, 145, June.

[5] H. Banerjee, M. Suhail, H. Ren, Biomimetics **2018**, 3, 3 15.

[6] L. Ionov, Materials Today **2014**, 17, 10 494.

[7] O. Erol, A. Pantula, W. Liu, D. H. Gracias, Advanced Materials Technologies **2019**, 4, 4 1.

[8] X. Zhou, T. Li, J. Wang, F. Chen, D. Zhou, Q. Liu, B. Li, J. Cheng, X. Zhou, B. Zheng, ACS Applied Materials & Interfaces **2018**, 10, 10 9077, pMID: 29465225.

[9] Y. Klein, E. Efrati, E. Sharon, Science **2007**, 315, 5815 1116.

[10] J. Kim, J. A. Hanna, M. Byun, C. D. Santangelo, R. C. Hayward, Science **2012**, 335, 6073 1201.

[11] C. Ma, X. Le, X. Tang, J. He, P. Xiao, J. Zheng, H. Xiao, W. Lu, J. Zhang, Y. Huang, T. Chen, Advanced Functional Materials **2016**, 26, 47 8670.

[12] R. M. Erb, J. S. Sander, R. Grisch, A. R. Studart, Nature Communications **2013**, 4 1.

[13] L. Huang, R. Jiang, J. Wu, J. Song, H. Bai, B. Li, Q. Zhao, T. Xie, Advanced Materials **2017**, 29, 7 1.

[14] S. Y. Zheng, Y. Shen, F. Zhu, J. Yin, J. Qian, J. Fu, Z. L. Wu, Q. Zheng, Advanced Functional Materials **2018**, 28, 37 1.

[15] Z. L. Wu, M. Moshe, J. Greener, H. Therien-Aubin, Z. Nie, E. Sharon, E. Kumacheva, Nature Communications **2013**, 4 1.

[16] L. Liu, S. Jiang, Y. Sun, S. Agarwal, Advanced Functional Materials **2016**, 26, 7 1021.

[17] S. Palagi, A. G. Mark, S. Y. Reigh, K. Melde, T. Qiu, H. Zeng, C. Parmeggiani, D. Martella, A. Sanchez-Castillo, N. Kapernaum, F. Giesselmann, D. S. Wiersma, E. Lauga, P. Fischer, Nature Materials **2016**, 15, 6 647.

[18] A. Mourran, H. Zhang, R. Vinokur, M. Möller, Advanced Materials **2017**, 29, 2.

[19] M. Y. Choi, Y. Shin, H. S. Lee, S. Y. Kim, J. H. Na, Scientific Reports **2020**, 10, 1 1.

[20] W. R. Frontera, J. Ochala, Calcified tissue international **2015**, 96, 3 183.

[21] M. Drost, M. Maenhout, P. Willems, C. Oomens, F. Baaijens, M. Hesselink, Journal of biomechanics **2003**, 36, 7 1055.

[22] F. Buchthal, H. Schmalbruch, Physiological reviews **1980**, 60, 1 90.

[23] W. M. KIER, K. K. SMITH, Zoological Journal of the Linnean Society **1985**, 83, 4 307.

[24] W. M. Kier, F. H. Schachat, The Journal of experimental biology **1992**, 168 41.

[25] Z. Liu, M. A. Meyers, Z. Zhang, R. O. Ritchie, Progress in Materials Science **2017**, 88 467.

[26] S. Hanassy, A. Botvinnik, T. Flash, B. Hochner, Bioinspiration & Biomimetics 10, 3 1.

[27] A. Kazakidi, D. P. Tsakiris, D. Angelidis, F. Sotiropoulos, J. A. Ekaterinaris, Computers and Fluids **2015**, 115 54.

[28] J. N. Richter, B. Hochner, M. J. Kuba **2015**, 1069–1076.

[29] R. Yagel, D. Cohen, Computer **1993**, 26, 7 51.

[30] J. Hiller, H. Lipson, Rapid Prototyping Journal **2010**, 16, 4 241.

[31] N. Oxman, Virtual and Physical Prototyping **2011**, 6, 1 3.

[32] G. Sossou, F. Demoly, H. Belkebir, H. J. Qi, S. Gomes, G. Montavon, Materials and Design **2019**, 175 107798.

[33] N. Cheney, R. MacCurdy, J. Clune, H. Lipson, ACM SIGEVOlution **2014**, 7, 1 11.

[34] J. Hiller, H. Lipson, Rapid Prototyping Journal **2009**, 15, 2 137.

[35] Proceedings of the National Academy of Sciences of the United States of America **2020**, 117, 4 1853.

[36] C. Yu, Z. Duan, P. Yuan, Y. Li, Y. Su, X. Zhang, Y. Pan, L. L. Dai, R. G. Nuzzo, Y. Huang, H. Jiang, J. A. Rogers, Advanced Materials **2013**, 25, 11 1541.

[37] X. Z. Zhang, X. D. Xu, S. X. Cheng, R. X. Zhuo, Soft Matter **2008**, 4, 3 385.

[38] A. B. Imran, T. Seki, Y. Takeoka, Polymer Journal **2010**, 42, 11 839.

[39] S. Kim, K. Lee, C. Cha, Journal of Biomaterials Science, Polymer Edition **2016**, 27, 17 1698.

[40] D. Gan, L. A. Lyon, Journal of the American Chemical Society **2001**, 123, 31 7511.

[41] P. Li, X. Hou, L. Qu, X. Dai, C. Zhang, Polymers **2018**, 10, 2.

[42] K. Depa, A. Strachota, M. Šlouf, J. Hromádková, European Polymer Journal **2012**, 48, 12 1997.

[43] C. Ma, T. Li, Q. Zhao, X. Yang, J. Wu, Y. Luo, T. Xie, Advanced Materials **2014**, 26, 32 5665.

[44] E. Otsuka, S. Komiya, S. Sasaki, J. Xing, Y. Bando, Y. Hirashima, M. Sugiyama, A. Suzuki, Soft Matter **2012**, 8, 31 8129.

[45] N. Bodenberger, D. Kubiczek, I. Abrosimova, A. Scharm, F. Kipper, P. Walther, F. Rosenau, Biotechnology Reports **2016**, 12 6.

[46] A. Pica, G. Graziano, Physical Chemistry Chemical Physics **2016**, 18, 36 25601.

[47] Q. Wang, C. S. Biswas, M. Galluzzi, Y. Wu, B. Du, F. J. Stadler, RSC Advances **2017**, 7, 15 9381.

[48] W.-F. Lee, S.-H. Yen, Journal of Applied Polymer Science **2000**, 78, 9 1604.

[49] X. Zhang, R. Zhuo, Y. Yang **2002**, 23 1313.

[50] Q. Feng, L. Z. Du, Q. Z. Yan, C. C. Ge, Advanced Materials Research **2011**, 295-297 1193.

[51] H. Tokuyama, N. Ishihara, S. Sakohara, Polymer Bulletin **2008**, 61, 3 399.

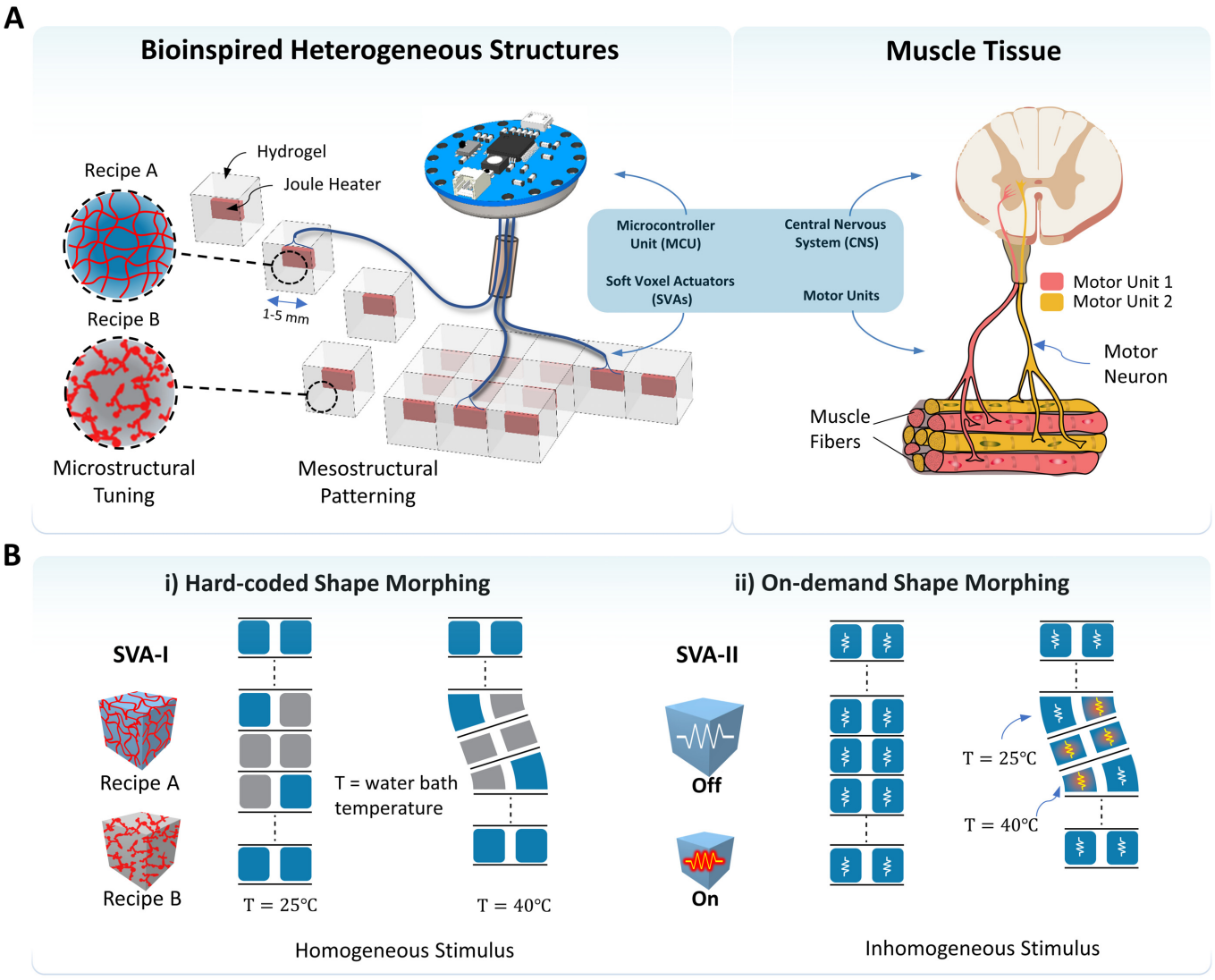

Figure 1: Illustration of bioinspired heterogeneous hydrogel structures composed of tunable and addressable voxels. **A)** Soft Voxel Actuators (SVAs) are electrically addressable building blocks whose deformations can be controlled by a microcontroller unit (MCU). SVAs are analogous to motor units, consisting of a motor neuron and associated muscle fibers, which deform in response to electrical impulses from the CNS. The microstructure of the hydrogels used to make SVAs can be altered, resulting in tunable material properties. **B)** i) SVAs without embedded Joule heaters (SVA-I) are used to create structures with hard-coded shape morphing that respond to a homogeneous temperature field acting globally on the entire structure through the surrounding water bath. ii) SVAs with embedded heaters (SVA-II) are used to create structures with on-demand shape morphing by forming an inhomogeneous temperature field throughout the structure.

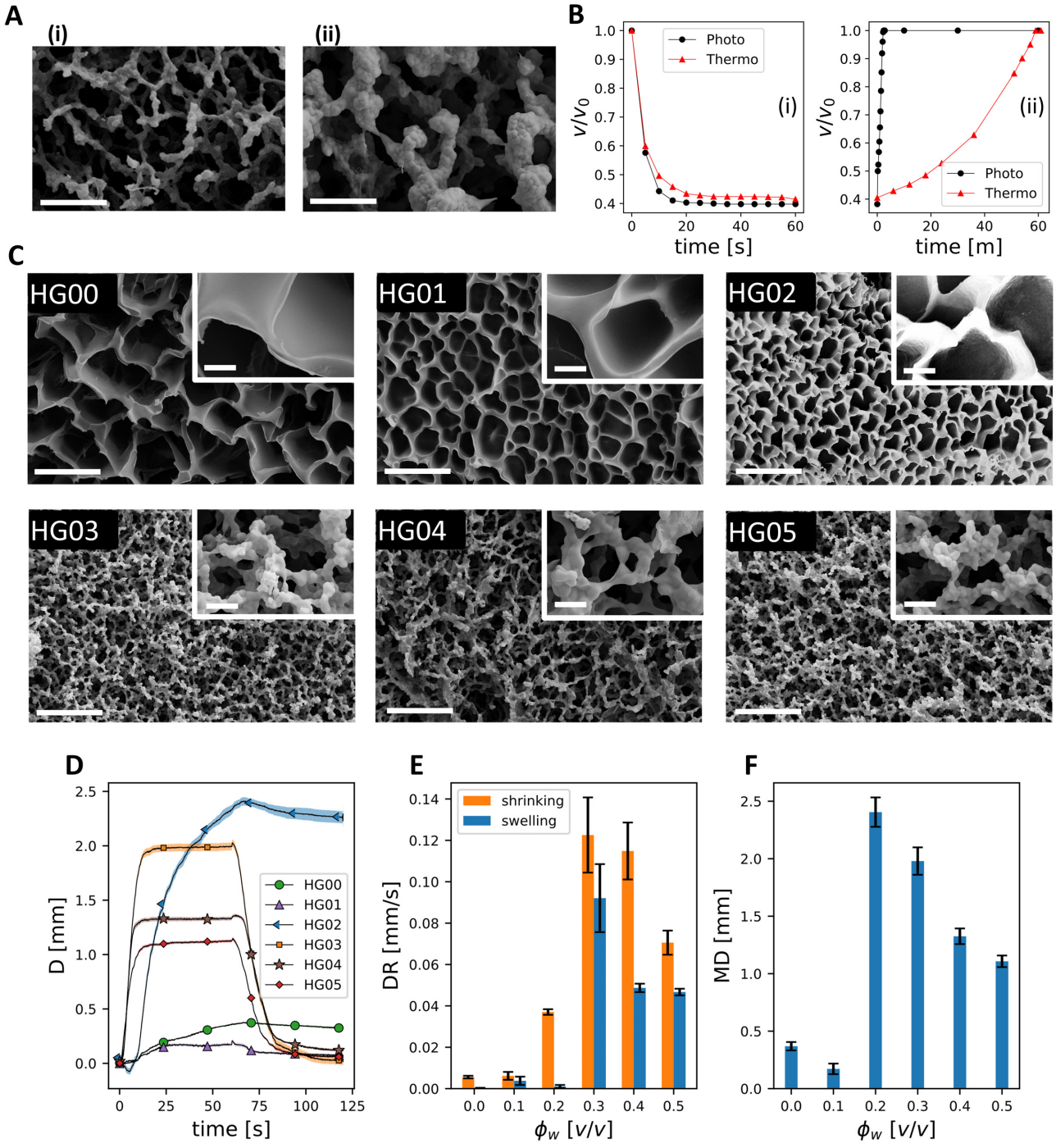

Figure 2: Tunable material properties using mixed solvent photopolymerization. **A)** SEM micrographs of photopolymerized (i) and thermopolymerized (ii) hydrogels synthesized in water volume fraction $\varphi_w = 0.27$ (scale bar $= 5\,\mu m$). **B)** Deswelling (i) and swelling (ii) rates of photopolymerized and thermopolymerized hydrogels synthesized in water volume fraction $\varphi_w = 0.27$. **C)** SEM images showing the effect of φ_w on pore structure of the photopolymerized PNIPAAm hydrogel (scale bars $10\,\mu m$ and $1\,\mu m$ for low and high magnification, respectively). **D)** Displacement (D) over time generated by SVA-II units with different values of φ_w under a $1\,gf$ load, as measured by the setup described in the Supporting Information. **E,F)** Displacement rate (DR) and maximum displacement (MD) of SVA-II units as a function of φ_w,(extracted from B as described in the Supporting Information).

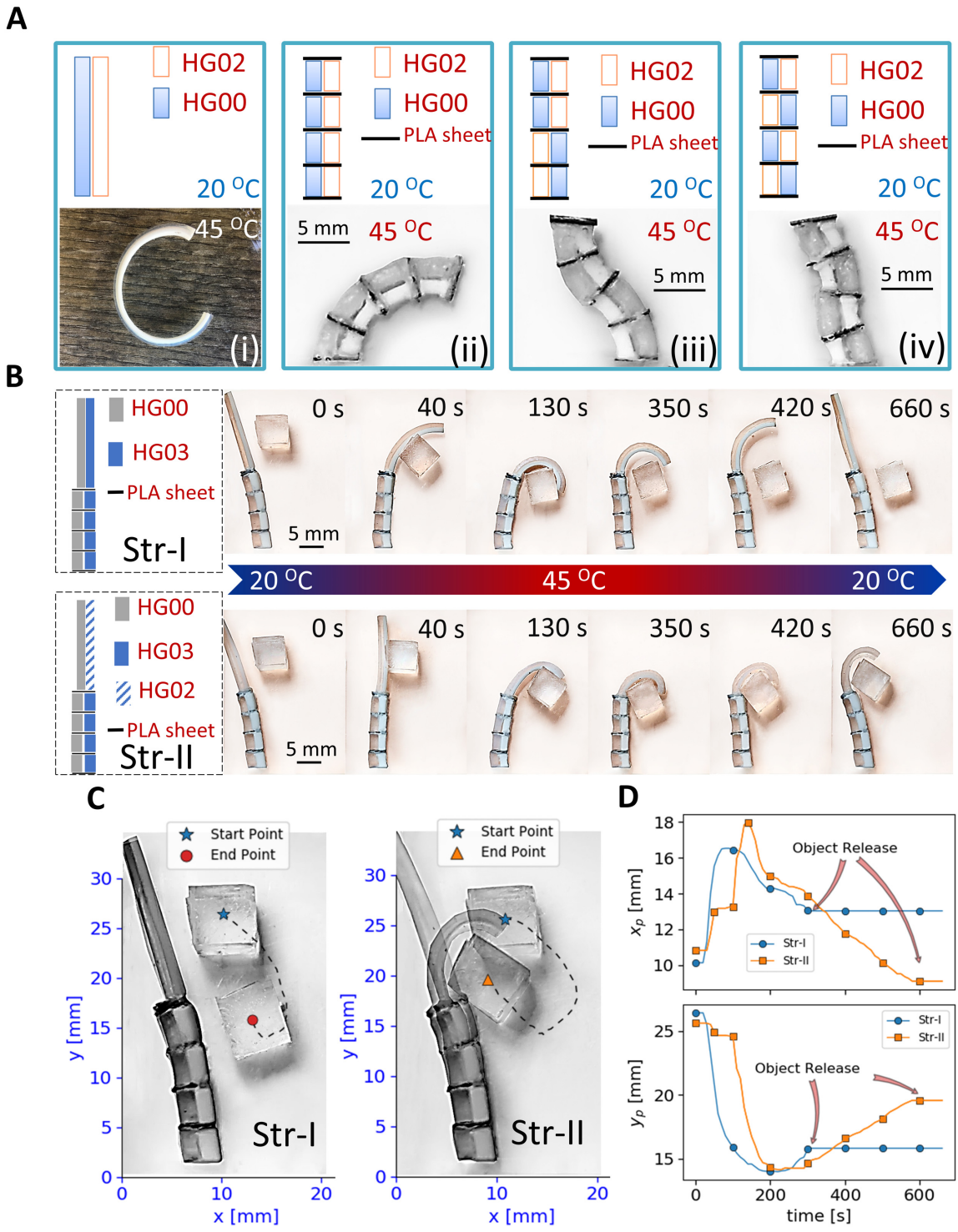

Figure 3: Realization of structural inhomogeneity through patterning of hydrogels with different swelling properties. **A)** (i) A two-material, two-region structure can almost bend into a circle when the surrounding water bath temperature is raised above the transition temperature of PNIPAAm hydrogel (32 °C) (ii-iv) Increasing the number of material domains in the structure enables it to achieve more diverse shapes. When the surrounding water bath temperature is increased, each structure reconfigures into a different shape, depending on its arrangement of SVA-I units. **B)** Hybrid structures comprised of substructures with the SVA arrangements in A)(i,ii) are capable of manipulating objects. The material distribution in two example structures, denoted by Str-I and Str-II, is shown in the schematic on the far left. The snapshots display the configurations of the two structures over time as the global water bath temperature is increased and then decreased. **C)** Image showing the start position, end position, and trajectory of the object manipulated by Str-I (left) and Str-II (right). **D)** Time evolution of the x and y coordinates of the manipulated object's center of mass. Str-I releases the object a $t = 300$ s, while Str-II releases it at $t = 600$ s, demonstrating the versatility of the voxel-based assembly approach to creating heterogeneous structures with diverse functions.

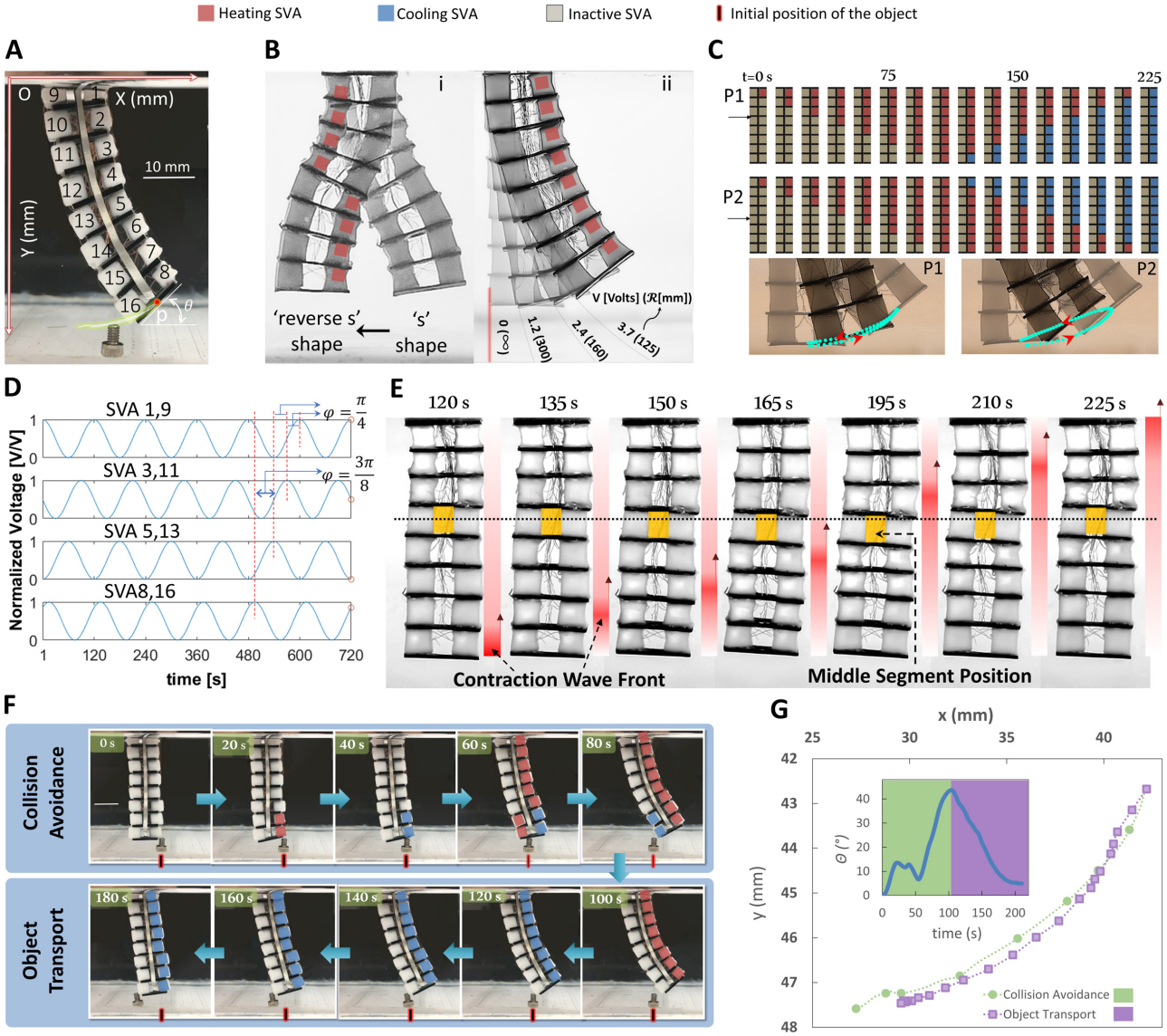

Figure 4: A miniature heterogeneous structure consisting of 16 addressable SVA-II units. **A)** SVA numbering scheme and the coordinate system used to measure the position of the point p and the angle θ of the end plate. **B)** On-demand shape morphing of the structure. i) The structure morphs from an 'S' shape to a 'reverse S' shape when particular SVAs are activated. ii) The structure's radius of curvature ($\mathcal{R}$) depends on the activation voltage (V) applied to SVAs 1-8. **C)** Dynamic shape changes are implemented by sequentially activating SVAs. In this case, SVAs 1 through 8 are activated according to the patterns labeled P1 and P2. The trajectory followed by the tip of the structure (shown at the bottom) can thus be adjusted on-demand. For details, see Movie S6 in the Supporting Information. **D)** Normalized sinusoidal voltages used to create longitudinal traveling waves in the structure. The voltages applied to 8 of the 16 SVAs are shown here. The SVAs are activated in pairs, and the voltage applied to each SVA pair is $\frac{\pi}{8}$ *rad* out of phase with respect to the voltage applied to the next active pair. **E)** The longitudinal traveling wave as it propagates through the structure. One SVA pair, indicated by the yellow square, is kept inactive in order to serve as a reference point. For details, refer to Movie S7 in the Supporting Information. **F)** Example usage of heterogeneous structures with on-demand control of deformation. The structure can avoid collisions with objects or transport them, depending on the sequence of voltage commands from the microcontroller unit. **G)** Trajectory of the point p on the tip of the structure as it first avoids and then transports the object. The inset shows the angle θ of the end plate as a function of time.